The following publication Tao Gui, Chao Lu, Alan Pak Tao Lau, and P. K. A. Wai, "High-order modulation on a single discrete eigenvalue for optical communications based on nonlinear Fourier transform," Opt. Express 25, 20286-20297 (2017) is available at https://doi.org/10.1364/OE.25.020286.

Research Article | Vol. 25, No. 17 | 21 Aug 2017 | OPTICS EXPRESS 20286

Optics EXPRESS

High-order modulation on a single discrete eigenvalue for optical communications based on nonlinear Fourier transform

Tao Gui,[1,*] Chao Lu,[2] Alan Pak Tao Lau,[1] and P. K. A. Wai[2]

[1]*Photonics Research Centre, Department of Electrical Engineering, The Hong Kong Polytechnic University, Hung Hom, Kowloon, Hong Kong*

[2]*Photonics Research Centre, Department of Electronic and Information Engineering, The Hong Kong Polytechnic University, Hung Hom, Kowloon, Hong Kong*

**15900594r@connect.polyu.hk*

Abstract: In this paper, we experimentally investigate high-order modulation over a single discrete eigenvalue under the nonlinear Fourier transform (NFT) framework and exploit all degrees of freedom for encoding information. For a fixed eigenvalue, we compare different 4 bit/symbol modulation formats on the spectral amplitude and show that a 2-ring 16-APSK constellation achieves optimal performance. We then study joint spectral phase, spectral magnitude and eigenvalue modulation and found that while modulation on the real part of the eigenvalue induces pulse timing drift and leads to neighboring pulse interactions and nonlinear inter-symbol interference (ISI), it is more bandwidth efficient than modulation on the imaginary part of the eigenvalue in practical settings. We propose a spectral amplitude scaling method to mitigate such nonlinear ISI and demonstrate a record 4 GBaud 16-APSK on the spectral amplitude plus 2-bit eigenvalue modulation (total 6 bit/symbol at 24 Gb/s) transmission over 1000 km.

© 2017 Optical Society of America

OCIS codes: (060.2330) Fiber optics communications; (070.4340) Nonlinear optical signal processing.

References and links

1. E. G. Turitsyna and S. K. Turitsyn, "Digital signal processing based on inverse scattering transform," Opt. Lett. **38**(20), 4186–4188 (2013).
2. J. E. Prilepsky, S. A. Derevyanko, and S. K. Turitsyn, "Nonlinear spectral management: Linearization of the lossless fiber channel," Opt. Express **21**(20), 24344–24367 (2013).
3. M. I. Yousefi and F. R. Kschischang, "Information Transmission using the Nonlinear Fourier Transform, Part I: Mathematical Tools," IEEE Trans. Inf. Theory **60**(7), 4312–4328 (2014).
4. M. I. Yousefi and F. R. Kschischang, "Information Transmission using the Nonlinear Fourier Transform, Part II: Numerical Methods," IEEE Trans. Inf. Theory **60**(7), 4329–4345 (2014).
5. M. I. Yousefi and F. R. Kschischang, "Information Transmission using the Nonlinear Fourier Transform, Part III: Spectrum Modulation," IEEE Trans. Inf. Theory **60**(7), 4346–4369 (2014).
6. S. A. Derevyanko, J. E. Prilepsky, and S. K. Turitsyn, "Capacity estimates for optical transmission based on the nonlinear Fourier transform," Nat. Commun. **7**, 12710 (2016).
7. S. K. Turitsyn, J. E. Prilepsky, S. T. Le, S. Wahls, L. L. Frumin, M. Kamalian, and S. A. Derevyanko, "Nonlinear Fourier transform for optical data processing and transmission: advances and perspectives," Optica **4**(3), 307–322 (2017).
8. M. J. Ablowitz, D. J. Kaup, A. C. Newell, and H. Segur, "The inverse scattering transform Fourier analysis for nonlinear problems," Stud. Appl. Math. **53**(4), 249–315 (1974).
9. L. F. Mollenauer and J. P. Gordon, *Solitons in Optical Fibers: Fundamentals and Applications* (Academic, 2006).
10. A. Hasegawa, Y. Kodama, and A. Maruta, "Recent Progress in Dispersion-Managed Soliton Transmission Technologies," Opt. Fiber Technol. **3**, 197–213 (1997).
11. A. Hasegawa and Y. Kodama, *Solitons in Optical Communications* (Oxford University Press, 1995).
12. A. Hasegawa and T. Nyu, "Eigenvalue communication," IEEE J. Lightwave Technol **11**(3), 395–399 (1993).
13. O. V. Yushkoa, A. A. Redyuk, M. P. Fedoruk, and S. K. Turitsyn, "Coherent Soliton Communication Lines," Exper. Theor. Phys. **119**(5), 787–794 (2014).
14. H. Terauchi and A. Maruta, "Eigenvalue Modulated Optical Transmission System Based on Digital Coherent Technology," in *Opto-Electronics and Communications Conference* (OECC 2013), paper WR2–5.

#298175 https://doi.org/10.1364/OE.25.020286
Journal © 2017 Received 15 Jun 2017; revised 8 Aug 2017; accepted 8 Aug 2017; published 11 Aug 2017

© 2017 Optica Publishing Group. Users may use, reuse, and build upon the article, or use the article for text or data mining, so long as such uses are for non-commercial purposes and appropriate attribution is maintained. All other rights are reserved.

Optics EXPRESS

15. Y. Matsuda, H. Terauchi, and A. Maruta, "Design of Eigenvalue-multiplexed Multi-level Modulation Optical Transmission System," in *Opto-Electronics and Communications Conference* (OECC 2014), pp. 1016–1018
16. Z. Dong, S. Hari, T. Gui, K. Zhong, M. Yousefi, C. Lu, P. K. A. Wai, F. R. Kschischang, and A. P. T. Lau, "Nonlinear Frequency Division Multiplexed Transmissions based on NFT," IEEE Photonics Technol. Lett. **27**(15), 1621–1623 (2015).
17. V. Aref, H. Bülow, K. Schuh, and W. Idler, "Experimental Demonstration of Nonlinear Frequency Division Multiplexed Transmission," in *European Conference on Optical Communication* (ECOC 2015), paper Tu 1.1.2.
18. H. Bülow, V. Aref, and W. Idler, "Transmission of waveforms determined by 7 eigenvalues with PSK-modulated spectral amplitudes," in *European Conference on Optical Communication* (ECOC 2016), paper Tu3E.2.
19. S. T. Le, I. D. Phillips, J. E. Prilepsky, P. Harper, A. D. Ellis, and S. K. Turitsyn, "Demonstration of Nonlinear Inverse Synthesis Transmission Over Transoceanic Distances," IEEE J. Lightwave Technol. **34**(10), 2459–2466 (2016).
20. S. T. Le, I. D. Phillips, J. E. Prilepsky, M. Kamalian, A. D. Ellis, P. Harper, and S. K. Turitsyn, "Achievable information rate of nonlinear inverse synthesis based 16QAM OFDM transmission," in *European Conference on Optical Communication* (ECOC 2016), paper Th.2.P2.SC5.
21. S. T. Le, H. Buelow, and V. Aref, "Demonstration of 64x0.5Gbaud Nonlinear Frequency Division Multiplexed Transmission with 32QAM," in *Optical Fiber Communication Conference* (OFC 2017), paper W3J.1.
22. V. Aref, T. Le Son, and H. Buelow, "Demonstration of Fully Nonlinear Spectrum Modulated System in the Highly Nonlinear Optical Transmission Regime," in *European Conference on Optical Communication* (ECOC 2016), paper Th.3.B.2.
23. T. Gui, S. K. Lo, X. Zhou, C. Lu, A. P. T. Lau, and P. K. A. Wai, "4 bits/symbol Phase and Amplitude Modulation on a Single Discrete Eigenvalue for Nonlinear Fourier Transform based Transmissions," in *Optical Fiber Communication Conference* (OFC 2017), paper Th2A.58.
24. V. E. Zakharov and A. B. Shabat, "Exact theory of 2-dimensional self-focusing and one dimensional self-modulation of waves in nonlinear media," Sov. Phys. JETP **34**, 62–69 (1972).
25. M. J. Ablowitz and H. Segur, *Solitons and the inverse scattering transform* (SIAM, 1981).
26. T. Gui, T. H. Chan, C. Lu, A. P. T. Lau, and P. K. A. Wai, "Alternative decoding methods for optical communications based on nonlinear Fourier transform," IEEE J. Lightwave Technol. **35**(9), 1542–1550 (2017).
27. V. B. Matveev and M. A. Salle, *Darboux transformations and solitons* (Springer, 1991).
28. S. Hari and F. R. Kschischang, "Bi-Directional Algorithm for Computing Discrete Spectral Amplitudes in the NFT," IEEE J. Lightwave Technol. **34**(15), 3529 (2016).
29. Q. Zhang and T. Chan, "A Gaussian noise model of spectral amplitudes in soliton communication systems," in *IEEE 16th International Workshop on Signal Processing Advances in Wireless Communications* (SPAWC, 2015), pp. 455–459.
30. J. P. Gordon and H. A. Haus, "Random walk of coherently amplified solitons in optical fiber transmission," Opt. Lett. **11**(10), 665–667 (1986).
31. N. A. Shevchenko, e al. "A Lower Bound on the per Soliton Capacity of the Nonlinear Optical Fibre Channel," *in IEEE Information Theory Workshop* (ITW 2015), pp. 104–108.
32. S. A. Derevyanko, S. K. Turitsyn, and D. A. Yakushev, "Non-Gaussian Statistics of an Optical Soliton in the Presence of Amplified Spontaneous Emission," Opt. Lett. **28**(21), 2097–2099 (2003).
33. G. E. Falkovich, I. Kolokolov, V. Lebedev, and S. K. Turitsyn, "Statistics of soliton-bearing systems with additive noise," Phys. Rev. E **63**, 025601 (2001).
34. S. A. Derevyanko, S. K. Turitsyn, and D. A. Yakushev, "Fokker-Plank equation approach to the description of soliton statistics in optical fiber transmission systems," J. Opt. Soc. Am. B **22**(4), 743 (2005).
35. S. Hari, *Fiber-optic Communication using Discrete Spectral Modulation [D]. University of Toronto (2016). https://*tspace.library.utoronto.ca/handle/1807/76449.
36. E. Iannone, F. Matera, A. Mecozzi, and M. Settembre, *Nonlinear optical communication networks* (Verlag-Wiley, 1998), pp. 156–159.

1. Introduction

Optical communications based on the nonlinear Fourier transform (NFT) has gained recent attention as a new theoretical framework for nonlinear fiber communications [1–7]. The NFT describes the optical signal propagated in the ideal Nonlinear Schrodinger Equation (NLSE) by a nonlinear spectrum (or eigenvalues) [8] and results in a simple linear channel transfer function without mutual interference. The nonlinear spectrum (or eigenvalues) λ is divided into 2 parts: the *continuous spectrum* where λ is real (corresponding to the "dispersive" signal components) and the *discrete spectrum* where λ lies on the upper-half complex plane (corresponding to the "solitonic" signal components). In the simplest case of fundamental soliton (i.e., solitons with one discrete eigenvalue), the pulses propagate through the fiber without changing their spectral and temporal shapes. Because of this unique feature, replacing the traditional return-to-zero (RZ) pulses with the soliton pulses can help to mutually

Optics EXPRESS

compensate the dispersion and nonlinear effects and significant progress in the field of soliton transmission was achieved in the 1990s [9–11]. However, most of the achievements were based on on-off keying detection even though the more general concept of 'eigenvalue communication' was also proposed by Hasagawa et al [12]. Following the advances of coherent detection technology in the last decade, arbitrarily complex signals can be generated and received, thus more dimensions can be used in NFT communication design. Simulation studies of coherent 1-soliton communication [13], eigenvalues transmission with digital coherent transceivers [14] and eigenvalue multiplexing transmission [15] illustrated their potential performance with present-day transceiver technologies. Recent experimental results demonstrated transmission and detection of independent modulation of 3 and 4 discrete eigenvalues [16]. Spectral amplitudes modulation on the eigenvalues such as independent QPSK modulation on 2 eigenvalues is reported in [17], followed by QPSK on 7 discrete eigenvalues [18]. On the other hand, experimental studies of continuous spectral modulation is currently underway [19–21] and most recently a demonstration of joint continuous and discrete spectrum modulation is reported in [22]. While continuous spectrum better resembles regular OFDM subcarriers in linear systems and higher order modulation formats can be easily realized, discrete spectral modulation or solitonic transmissions are mostly limited to QPSK format with 2 bits per symbol [17,18].

In this paper, we extend our previous work [23] on 4 bit/symbol modulation on a single discrete eigenvalue (or 1-soliton transmission) and conduct a thorough comparison and optimization of the constellation design to extend the transmission distance. We then exploit all available degrees-of-freedom for a 1-soliton system and demonstrate joint eigenvalue, phase and amplitude modulation that further increases the modulation order to 6 bit/symbol. Modulation on the real part of the eigenvalue is found to outperform modulation on the imaginary part of the eigenvalue. Meanwhile, pulse timing drift and nonlinear ISI caused by eigenvalue modulation is theoretically analyzed and a timing pre-shift method is proposed to mitigate such effects. A record 4 GBaud, 6 bit/symbol with total bit rate 24 Gb/s transmission over 1000 km is achieved for discrete eigenvalue modulated NFT systems.

The rest of the paper is organized as follows. A brief introduction of the NFT framework, DSP strategy and experimental setup is given in Section 2. In Section 3, we study various 4 bit/symbol modulation formats on the spectral amplitude of a fixed discrete eigenvalue and derive optimal constellation designs in experimental settings. Section 4 gives the joint spectral phase, spectral magnitude and eigenvalue modulation, and derives the corresponding signal processing techniques to achieve 4 GBaud, 6 bit/symbol transmissions with extended reach. Conclusions will be drawn in Section 5.

2. Signal processing strategy and experimental setup

The NFT of a signal $q(t)$ (in normalized units), supported in the interval $[T_1,T_2]$, is defined by solving the differential equation [24]

$$\frac{\mathrm{d}v}{\mathrm{d}t}=\begin{pmatrix}-j\lambda & q(t)\\ -q^*(t) & j\lambda\end{pmatrix}v,\ v(T_1,\lambda)=\begin{pmatrix}v_1(T_1,\lambda)\\ v_2(T_1,\lambda)\end{pmatrix}=\begin{pmatrix}1\\0\end{pmatrix}e^{-j\lambda T_1} \tag{1}$$

where λ and $v(t,\lambda)$ are, respectively, the eigenvalue and eigenvector. Let $a(\lambda)=v_1(T_2,\lambda)e^{j\lambda T_2}$ and $b(\lambda)=v_2(T_2,\lambda)e^{-j\lambda T_2}$. For discrete eigenvalue systems, the NFT of $q(t)$ is defined as $\tilde{q}(\lambda)=b(\lambda)/a'(\lambda)$ (where $a'(\lambda)=da(\lambda)/d\lambda$) at isolated roots $a(\lambda_{rt})=0$ in the upper-half complex plane. The set of isolated roots $\lambda_{rt}\in\mathbb{C}^+$ are called discrete eigenvalues and the NFT $\tilde{q}(\lambda_{rt})$ is also referred to as the spectral amplitude. When there is only one eigenvalue $\lambda_{rt}=\lambda_R+j\lambda_I$, the signal $q(t)$ is also commonly known as a 1-

Optics EXPRESS

soliton. In this case, the closed form expression of $q(t)$ can be obtained by solving a Riemann-Hilbert system for the inverse NFT (INFT) [25] and the general time-domain waveform is given by

$$q(t) = -2j\lambda_I e^{-j\angle\tilde{q}(\lambda_{rt})}\operatorname{sech}\left(2\lambda_I\left(t-t_0\right)\right)e^{-2j\lambda_R t} \tag{2}$$

where $t_0 = \frac{1}{2\lambda_I}\ln\left(\frac{|\tilde{q}(\lambda_{rt})|}{2\lambda_I}\right)$ is the time-center of the signal, $\angle\tilde{q}(\lambda_{rt})$) is the spectral phase, and $|\tilde{q}(\lambda_{rt})|$ is the spectral magnitude. After propagation with *z*, the time-center of the pulse t_0 in (2) will evolve according to

$$t_0(z) = 4\lambda_R z + \frac{1}{2\lambda_I}\ln\left(\frac{|\tilde{q}(\lambda_{rt})|}{2\lambda_I}\right). \tag{3}$$

In the soliton transmission literature, one often describes solitons as having four degrees of freedom to encode information – the pulse amplitude (determined by λ_I), the frequency (determined by λ_R), the timing (determined by $|\tilde{q}(\lambda_{rt})|$) and the phase (determined by $\angle\tilde{q}(\lambda_{rt})$). Recent advances in digital coherent technologies open up completely new ways to efficiently exploit these 4 degrees of freedom and we will hereby describe information encoding in 1-solitons in terms of spectral phase $\angle\tilde{q}(\lambda_{rt})$), spectral magnitude $|\tilde{q}(\lambda_{rt})|$ and eigenvalue λ_{rt} modulation. Note that the $q(t)$ here is in normalized units and can be mapped into a physical time-domain signal $Q(\tau)$ by a change of the variables

$$Q = \sqrt{\frac{|\beta_2|}{\gamma T_0^2}}q, \quad \tau = T_0 t, \quad l = -\frac{T_0^2}{|\beta_2|}z \tag{4}$$

where T_0 is a free parameter related to pulse-width and physical bandwidth of the signal, β_2 is the group velocity dispersion coefficient, and γ is the fiber Kerr nonlinearity coefficient.

In our recent paper [26], we showed that for NFT systems employing spectral phase and magnitude modulation on a given discrete eigenvalue, $b(\lambda_{rt})$ already contains all the phase and amplitude information of $\tilde{q}(\lambda_{rt})$ and $a'(\lambda_{rt})$ just adds an unnecessary noise component. Thus, $b(\lambda_{rt})$ should be used as the decision statistic instead of $\tilde{q}(\lambda_{rt})$. Furthermore, it was also shown that the noise in $a'(\lambda_{rt})$ and the eigenvalue noise in λ_{rt} are all correlated with the noise in $b(\lambda_{rt})$ A corresponding linear minimum mean square error (LMMSE) estimator of the phase and amplitude noise in $b(\lambda_{rt})$ can be derived to obtain considerable transmission performance improvement [26].

Optics EXPRESS

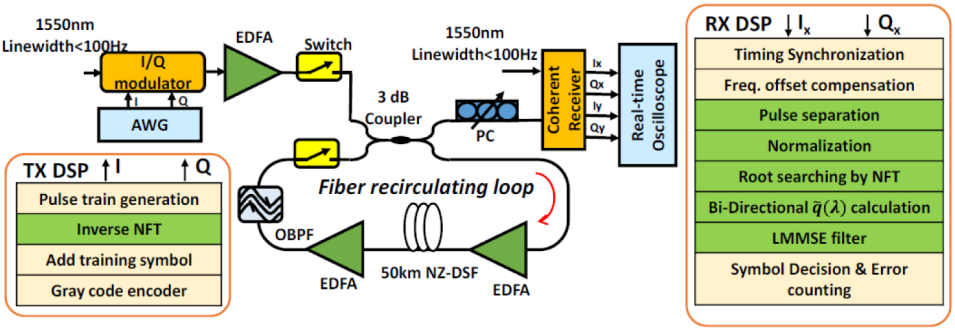

Fig. 1. DSP structure and experimental setup. AWG: arbitrary waveform generator; OBPF: optical band-pass filter; PC: polarization controller. NZ-DSF: non-zero dispersion shifted fiber.

Figure 1 shows the experimental setup for the NFT transmission system. The 1-soliton signals are recursively computed by inverse NFT which is based on the Darboux transformation method [27] (Alternatively, one can also simply generate the waveform according to (2) for this particular class of 1-soliton signals in our study). Around 65280 Gray coded-symbols are mapped onto the spectral phase, spectral magnitude and the location of the discrete eigenvalue. These waveforms are then generated in the arbitrary waveform generator (AWG) with 92 GSa/s and used to drive the IQ modulator. The output of the modulator is a train of optical soliton pulses, which are amplified and launched into a NZ-DSF fiber recirculating loop. The loop consists of 50-km spans and lumped amplification only by EDFA. Since the theory of NFT is based on the integrability property of the lossless NLS equation, this short fiber span length can largely reduce the penalty of fiber loss. A flat-top optical filter with a 3-dB bandwidth of 1 nm is used inside the loop to suppress the out-of-band amplified spontaneous emission (ASE) noise. Both the transmitter laser and local oscillator are from a single fiber laser source with very low laser phase noise (NKT Koheras ADJUSTIK Fiber laser with linewidth < 100Hz). After alignment by a polarization controller in the x-polarization, the received signal is then coherently detected and sampled by a digital storage scope with a sampling rate of 80 GSa/s and a bandwidth of 33 GHz. The sampled signal is analyzed by off-line digital signal processing (DSP), whose structure is also shown in Fig. 1. After timing synchronization and frequency offset compensation, the received signal samples are then separated in time blocks and normalized into discrete pulses followed by the NFT operation to search for the roots λ_{rt} where $a(\lambda_{rt})=0$. The Bi-Directional Algorithm of [28] is used to compute the spectral amplitudes $\tilde{q}(\lambda_{rt})$. The phase rotation of $\tilde{q}(\lambda_{rt})$ due to propagation and the LMMSE filter coefficients are first estimated by training symbols, then used to reduce the phase and magnitude noise of $b(\lambda_{rt})$. This is followed by symbol decisions and bit error ratio (BER) calculations.

3. 4 bit/symbol spectral phase and magnitude modulation on a single discrete eigenvalue

To illustrate the effectiveness of the proposed signal processing strategy using $b(\lambda_{rt})$ with LMMSE filter, we transmitted 4GBaud 1-soliton pulse trains on eigenvalue $\lambda_{rt}=0.3j$ with square 16-QAM on the phase and magnitude of the spectral amplitude $\tilde{q}(0.3j)$. Figure 2(a) shows the received signal distributions of $\tilde{q}(\lambda_{rt})$, $b(\lambda_{rt})$ and $b(\lambda_{rt})$ after the LMMSE filter and their corresponding BER as a function of transmission distance. One can clearly see that the $b(\lambda_{rt})$ after the LMMSE filter produces much cleaner distributions for symbol decisions which led to significant transmission reach extensions. Figure 2 (b) shows the BER versus the

Optics EXPRESS

number of training symbols used to estimate the LMMSE filter coefficients for a 800-km system. A mere 200 symbols are enough to accurately estimate the coefficients and hence one can conclude that the LMMSE filter is effective and induces minimal overhead. Therefore, we will only present and compare transmission performance based on $b(\lambda_{rt})$ with LMMSE filter for the rest of the paper.

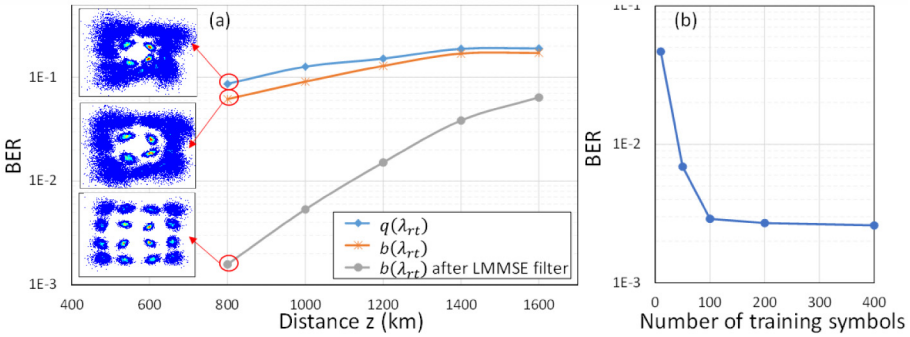

Fig. 2. 4GBaud square 16-QAM transmission on eigenvalue $\lambda_{rt} = 0.3j$. (a) Received signal distributions of $\tilde{q}(\lambda_{rt})$, $b(\lambda_{rt})$ and $b(\lambda_{rt})$ after the LMMSE filter and their corresponding BER performance versus transmission distance. (b) BER versus the number of training symbols for estimating the LMMSE filter coefficients for an 800-km system.

Unlike linear communications systems, additive white Gaussian noises (AWGN) from inline amplifiers do not decompose in a simple fashion in the nonlinear Fourier domain, and how noise will impact the discrete spectral amplitudes is generally unclear. Some preliminary studies [26,28–30] showed that perturbations of the spectral amplitudes $\tilde{q}(\lambda_{rt})$ can be modelled as Gaussian random variables but with different variances between the phase $\angle\tilde{q}(\lambda_{rt})$ and magnitude $|\tilde{q}(\lambda_{rt})|$. More accurate models in the soliton literatures [31–34] further showed that the Gaussian approximation will break down for long propagation distances. In this case, square 16-QAM modulation may not be optimal in NFT transmission systems. Thus we experimentally compared the performance of different 4 bit/symbol modulation formats such as 16-PSK (pure spectral phase modulation), 16-APSK (2-ring constellation) and square 16-QAM on eigenvalue $\lambda_{rt} = 0.3j$. Figure 3 (a) compares the transmission performance between these modulation formats and their received signal distributions after 1000 km transmission is also shown as insets. The baud rate is 4 Gbaud with a total bit rate of 16 Gb/s. The results obviously suggest that 16-APSK has the best performance while 16-PSK is the worst. Meanwhile, from the received signal distributions of 16-APSK, we noticed that the magnitude noise is stronger than phase noise and the phase distributions of received symbols are distinguishable but not the received magnitudes, which somewhat drives up the system BER. Therefore, the "distance" d between the two rings (as shown in the inset of Fig. 3 (b)) can be further optimized to improve performance. It should be emphasized that the "distance" here does not affect the amplitude hence power of the temporal signal waveform. Rather, changes in amplitudes of discrete spectral amplitude merely translate into temporal shift of the center of the pulse [26] as shown in the inset, which may cause neighboring pulse interference. Thus, a tradeoff exists between these two extremes. We performed a rough experimental investigation of system performance of 16-APSK with different "distance" d. The BER of 16-APSK with d = 1, 2, 3 and 4 versus distance are shown in Fig. 3(b). It appears that d = 3 gives optimal performance and the transmission reach can be extended to around 1400 km at BER = 2E-2.

Optics EXPRESS

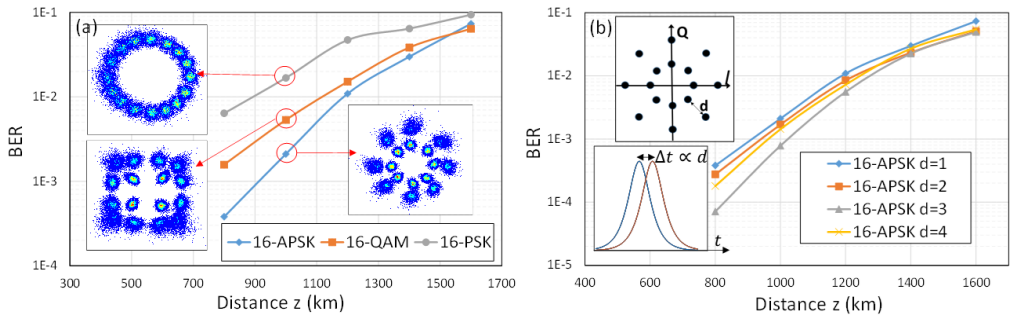

Fig. 3. BER versus distance of 4GBaud transmission on $\lambda_{rt} = 0.3j$ for (a) different 4 bit/symbol modulation formats (received signal distributions after 1000 km transmission are shown in the insets); (b) BER versus distance for 4GBaud 16-APSK transmissions with different *d* between the 2 rings.

We then characterized the effect of baud rate of the 16-APSK signals (with $d = 3$) up to 6 GBaud with a total bit rate of 24 Gb/s. Note that the baud rate of $Q(\tau)$ is only controlled by the free parameter T_0 in (3) where the symbol time in normalized units keeps constant. Figure 4(a) shows the signal amplitude $|Q(\tau)|$ with baud rate 2, 4 and 6 GBaud (the corresponding T_0 are 27.8 *ps*, 13.9 *ps*, and 9.3 *ps* respectively). With the increase in baud rate, the pulse width in physical units narrows down while the signal amplitude goes up. Figure 4(b) shows the physical spectrum of the 1-solitons with different baud rates. It can be seen that the 20-dB physical bandwidth are around 12, 24 and 48 GHz for 2, 4 and 6 GBaud respectively, which are considerably higher than those in linear systems with non-return-to-zero pulse shapes. The physical bandwidth of our setup is mainly limited by the 3dB analog bandwidth of AWG which is 32 GHz. Figure 4(c) compares the BER performance for various baud rates as a function of transmission distance. For 6 GBaud signals, a transmission reach of about 700 km for a soft-decision forward error correction (SD-FEC) threshold BER of 2E-2 can be obtained, while 2 GBaud signals can reach up to 2600 km for the same threshold. The trend of the BER curves implies that the performance of higher baud rate signal deteriorates faster with increasing transmission distance. The BER versus launched power at a certain transmission distance is also shown in Fig. 4(d), the optimal launched power of 6 GBaud signal is around 4 and 10 dB higher than that of 4 and 2 GBaud respectively, which is in good agreement with theoretical predictions according to (3). One can also observe that the higher baud rate signals are more sensitive to launched power fluctuations.

Optics EXPRESS

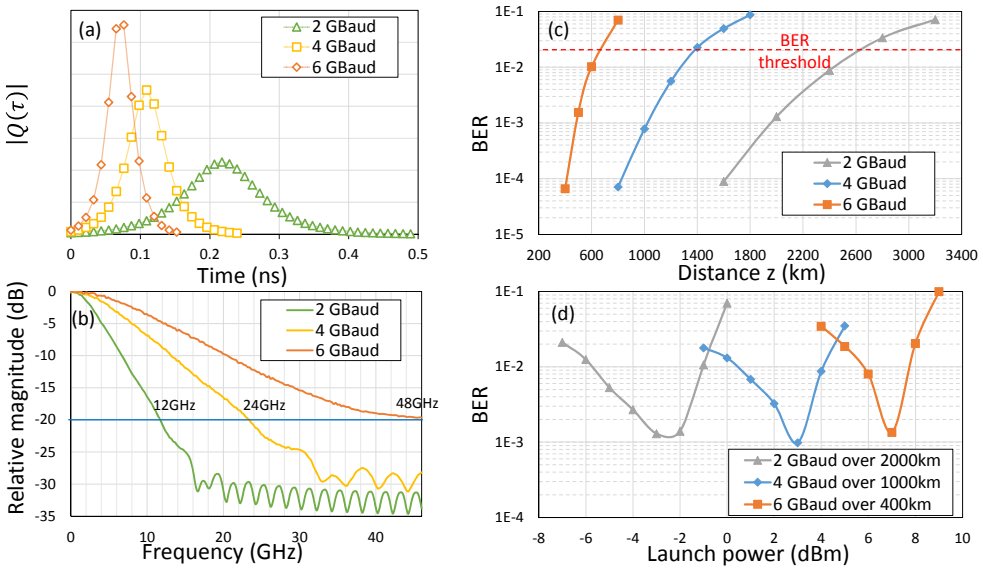

Fig. 4. Transmissions of 16-APSK (with $d = 3$) signals on $\lambda_{rt} = 0.3j$ with different baud rates; (a) Time-domain waveform $Q(\tau)$; (b) Frequency spectra; (c) BER versus transmission distance; (d) BER versus launched power for specific transmission distances

4. Joint spectral phase, spectral magnitude and eigenvalue modulation

Besides the phase and magnitude of spectral amplitudes $\tilde{q}(\lambda_{rt})$, the position of eigenvalue $\lambda_{rt} = \lambda_R + j\lambda_I$ in the upper complex plane is another degree of freedom for modulation. This joint modulation can be characterized as $(\lambda_k, \tilde{q}(\lambda_k))$ where λ_k belongs to the set $S = \{\lambda_1, \lambda_2, ...\lambda_N\}$ with N discrete eigenvalues. With M possible phase and magnitude combinations on $\tilde{q}(\lambda_k)$, the total number of bits per symbol of the system is further increased to $\log_2(N \times M)$. Note that in general λ_k is a not free choice in the whole upper complex plane. Rather, it should be bounded in a region determined by the available physical bandwidth and symbol interval for a given transmission distance, which was theoretically analyzed in [35]. Recall that from (3), modulating the real part of eigenvalue λ_R is equivalent to modulating the center frequency of the pulse, which will induce timing shift as a consequence of the group velocity difference. The timing shift grows with transmission distance which will result in pulse-to-pulse interaction and nonlinear inter-symbol interference (ISI) that ultimately limits transmission performance. On the other hand, modulating the imaginary part λ_I does not produce timing shifts but results in pulse compression or stretching that may dramatically broaden the physical bandwidth of the signal. Furthermore, it can be shown through perturbation theory that the noise variance of the imaginary part λ_I is 3 times more than that of real part λ_R [36], which means the noise tolerance in the λ_I dimension is much smaller than λ_R.

In this connection, we conduct a simple experimental comparison between the joint modulation with $\lambda_{rt} \in S_1 = \{-0.075 + 0.3j, 0.075 + 0.3j\}$ and $\lambda_{rt} \in S_2 = \{0.3j, 0.45j\}$. Both of the spacing between the 2 eigenvalues in the set S_1 and S_2 is equal to 0.15. Note that 16-APSK (with d = 3) are independently modulated on the spectral amplitude of the selected eigenvalues for each 1-soliton, which results in a total of 32 different pulses or 20 Gb/s with 5

Optics EXPRESS

bit/symbol. Figure 5 compares the 4 GBaud transmission performance of the 2 eigenvalue modulation strategies in terms of received signal distributions and BER. It is obvious that modulation on λ_R has a much better performance than that on λ_1. The empirical received distributions for $\lambda_{rt} \in S_1$ are more easily distinguishable from each other than that for $\lambda_{rt} \in S_2$. Note that the coefficients of the LMMSE filter are different for each λ_{rt}. Thus, error detection of λ_{rt} will introduce for the wrong LMMSE filter which may further enhance the noise of corresponding received spectral amplitudes $\tilde{q}(\lambda_{rt})$. That partly contributes to the degraded received distributions of $\tilde{q}(\lambda_{rt})$ for $\lambda_{rt} \in S_2$ when compared to that of S_1. Meanwhile, the inset at lower-left corner of Fig. 5 shows the physical spectrum of the two systems concerned. The 20-dB signal bandwidth of the $\lambda_{rt} \in \{0.3j, 0.45j\}$ signal is actually 10 GHz larger than the other one and exceeds the bandwidth of our setup, leading to more distortions as apparent in the received signal distributions. Moreover, note that for the $\lambda_{rt} \in \{-0.075+0.3j, 0.075+0.3j\}$ system, the pulse timing shift began to induce overlap between neighboring pulses and nonlinear ISI for 800 km transmission and above and dramatically degraded the BER performance. The comparisons show that modulating λ_R is more feasible and preferable than modulating λ_1 in our experiment setup. We note that one cannot draw such conclusion in general and a thorough theoretical and experimental comparisons between modulating λ_R and λ_1 are to be in place in future studies.

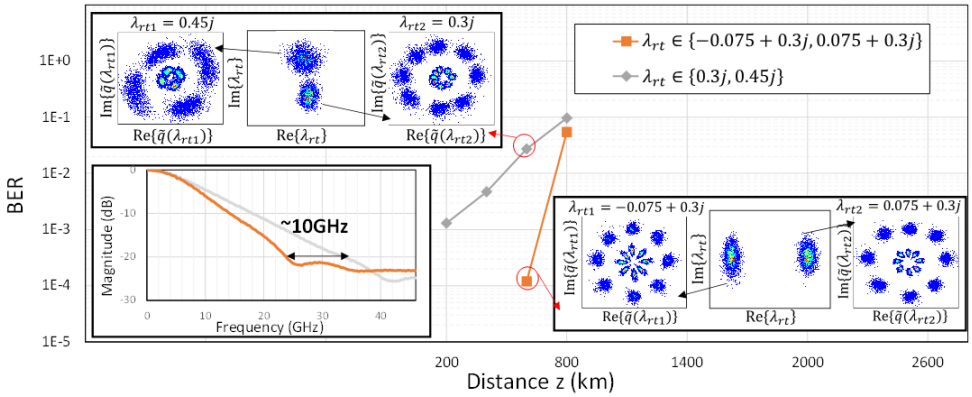

Fig. 5. BER versus distance of 4 GBaud transmissions of joint 16-APSK spectral amplitude modulation and eigenvalue modulation on $\lambda_{rt} = \{-0.075+0.3j, 0.075+0.3j\}$ and $\lambda_{rt} = \{0.3j, 0.45j\}$, frequency spectra and signal distributions over 600 km are shown as insets.

Driven by the insight above, we will focus on modulating λ_R in our investigation of joint spectral phase, magnitude and eigenvalue modulation. To reduce the impact of pulse timing drift and nonlinear ISI, we can pre-determine the timing of the transmitted pulse based on its corresponding eigenvalue so that the timing of the received pulse will still be within a given acceptable range. In particular, if we define $\Delta\tau$ as the maximum allowed time drift that the 99% of the pulse energy will still remain in the symbol time interval for pulse-by-pulse NFT processing, (3) becomes $t_0(l) = \left| -\frac{4\lambda_R |\beta_2|}{T_0^2} l + \frac{1}{2\lambda_I} ln\left(\frac{|\tilde{q}(\lambda)|}{2\lambda_I} \right) \right| \le \Delta\tau$. This inequality implies that the maximum transmission distance $l_{\max}$ should be smaller than

Optics EXPRESS

$$l_{\max} \le \begin{cases} \dfrac{\Delta\tau T_0^2}{4\lambda_R|\beta_2|} + \dfrac{T_0^2}{8\lambda_I\lambda_R|\beta_2|}\ln\left(\dfrac{\min\{|\tilde{q}(\lambda)|\}}{2\lambda_I}\right) & \lambda_R > 0 \\ \dfrac{\Delta\tau T_0^2}{4|\lambda_R\beta_2|} - \dfrac{T_0^2}{8\lambda_I|\lambda_R\beta_2|}\ln\left(\dfrac{\min\{|\tilde{q}(\lambda)|\}}{2\lambda_I}\right) & \lambda_R < 0 \end{cases} \tag{5}$$

Now, we can extend $l_{\max}$ by pre-shifting the pulse in the opposite direction at the transmitter so that the received pulse timing is still within $\Delta\tau$. This is illustrated in Fig. 6(b). The pre-shifting can be done by multiplying a different scaling factor α to $|\tilde{q}(\lambda_{rt})|$ depending on the sign of λ_R i.e. scaling the constellation of the spectral amplitude $\tilde{q}(\lambda_{rt})$ differently for different eigenvalues as shown in Fig. 6(c). For general spectral phase and magnitude modulation on $\tilde{q}(\lambda_{rt})$, the scaling factor α can be expressed as

$$\alpha = \begin{cases} \dfrac{2\lambda_I e^2 \lambda_I \Delta\tau}{\max\{|\tilde{q}(\lambda)|\}} & \lambda_R > 0 \\ \dfrac{2\lambda_I e^{-2\lambda_I\Delta\tau}}{\min\{|\tilde{q}(\lambda)|\}} & \lambda_R < 0 \end{cases} \tag{6}$$

and the corresponding maximum transmission distance is

$$l_{max} = \frac{\Delta\tau T_0^2}{2|\lambda_R\beta_2|} - \frac{T_0^2}{8\lambda_I|\lambda_R\beta_2|}\ln\left(\frac{\max\{|\tilde{q}(\lambda)|\}}{\min\{|\tilde{q}(\lambda)|\}}\right) \tag{7}$$

In particular, for systems with pure phase modulation on the spectral amplitude $\tilde{q}(\lambda_{rt})$, appropriate pre-shifting of the soliton pulse can double the maximum transmission distance $l_{\max}$ to $\dfrac{\Delta\tau T_0^2}{2|\lambda_R\beta_2|}$.

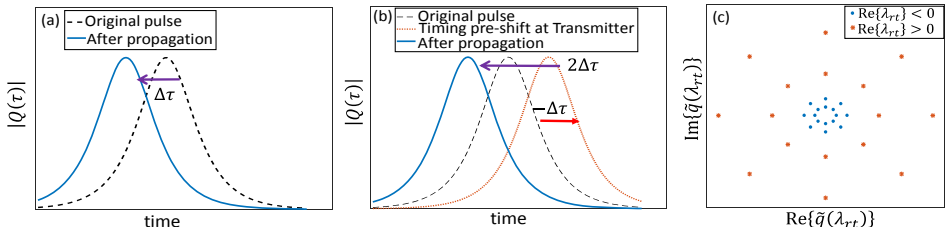

Fig. 6. (a) A 1-soliton pulse with eigenvalue $\lambda_{rt} = \lambda_R + j\lambda_I$ where $\lambda_R \neq 0$ will drift in time after propagation. (b) Pre-shifting the original pulse at the transmitter can enhance the amount of acceptable pulse drifting, thus increase the transmission distance. (c) 16-APSK constellation on the spectral amplitude $\tilde{q}(\lambda_{rt})$ of pre-shifted pulse for $\mathrm{Re}\{\lambda_{rt}\} > 0$ and $\mathrm{Re}\{\lambda_{rt}\} < 0$.

We adopted the method described above and attempted to transmit 4 GBaud 16-APSK (with $d = 3$) signals together with independent modulation on 4 different eigenvalues, giving a total 6 bit/symbol and aggregate bit rate of 24 Gb/s. The 4 eigenvalues are $\lambda_{rt} = \{-1.5\delta + 0.3j, -0.5\delta + 0.3j, 0.5\delta + 0.3j, 0.5\delta + 0.3j\}$. The choice of δ depends not only on eigenvalue noise but also the acceptable pulse drift for a given transmission distance. Note that the free parameter T_0 is 13.9 *ps*, and 99%-energy time-widths of the soliton pulses is 80% of the 250 *ps* (symbol period corresponding to a 4 Gbaud signal). Thus, the maximum

Optics EXPRESS

allowed time drift $\Delta\tau$ in physical units is derived to be 25 *ps*. With Eq. (7) and the typical value of dispersion coefficient $\beta_2 = -5.01\ ps^2km^{-1}$, we can theoretically estimate that $|\lambda_R|$ should be smaller than 0.12 and hence $|\delta| \le 0.08$ in order to guarantee negligible nonlinear ISI after transmission of 1000 *km* over NZ-DSF fiber. We then experimentally characterize the BER performance over 1000 km with δ from 0.05 to 0.08 and the results are shown in Fig. 7(a), which indicates that $\delta = 0.06$ is optimal. The empirical received eigenvalue distributions with $\delta = 0.06$ is also shown as the inset, which is quite distinguishable even after transmission of 1000 km.

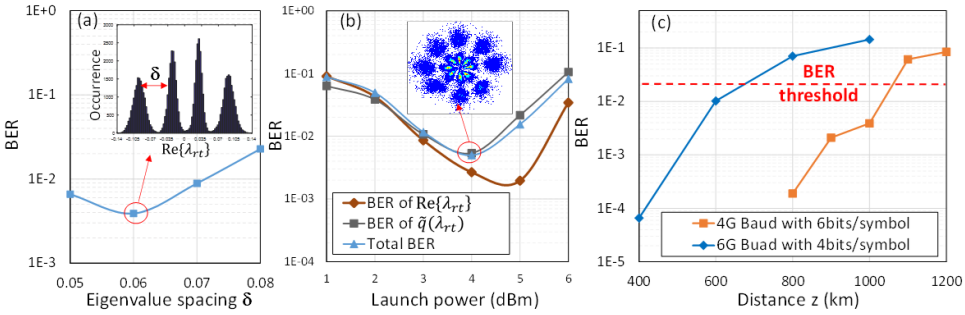

Fig. 7. Four GBaud 16-APSK transmission over 1000 km with 2-bit eigenvalue modulation from the set $\lambda_{rt} = \{-1.5\delta + 0.3j, -0.5\delta + 0.3j, 0.5\delta + 0.3j, 0.5\delta + 0.3j\}$ (a) BER versus eigenvalue spacing δ between $\mathrm{Re}\{\lambda_{rt}\}$ (received eigenvalue distributions shown in inset); (b) signal launched power versus BER; (c) BER comparison between 6 GBaud 16-APSK and 4 GBaud APSK with 2-bit eigenvalue modulation (total 24 Gb/s) system as a function of transmission distance.

Figure 7(b) shows the BER of $\mathbf{Re}\{\lambda_{rt}\}$, BER of $\tilde{\boldsymbol{q}}\{\lambda_{rt}\}$ and total BER as a function of launched power for a 1000-km system. The total BER of 6 bit/symbol signal is contributed to by both the eigenvalue decision errors and the decision errors of 16-APSK on each eigenvalues. Note that the BER of $\mathbf{Re}\{\lambda_{rt}\}$ continue to decline with the launched power until 5 dBm. Finally, we experimentally compare the BER performance for the two methods to realize 24 Gb/s transmission: 4 GBaud 16-APSK with 2-bit eigenvalue modulation (6 bit/symbol) and 6 Gbaud 16-APSK signals with no eigenvalue modulation (4 bit/symbol) as described in the last section and the results are shown in Fig. 7(c). For the SD-FEC threshold, the 6 bit/symbol system outperform the other by around 1050 km. To the best of our knowledge, this is the highest demonstrated bit rate, baud rate and modulation order for discrete spectral modulation under the NFT framework. Note that the abrupt increase of BER beyond 1000 km is caused by pulse drifting-induced nonlinear ISI. However, as the current eigenvalue spacing δ is optimized specifically for 1000-km transmission, one can further improve the overall transmission performance by choosing an appropriate δ for each distance that can achieve good tradeoffs between eigenvalue decision errors and nonlinear ISI. This will be one of the important topics to be studied in the future.

5. Conclusions

In this paper, we experimentally investigated joint modulation of spectral phase, spectral magnitude as well as eigenvalue for single discrete eigenvalue or 1-soliton transmission systems. We first considered a fixed eigenvalue and compared the performance of various 4 bit/symbol modulation formats on the spectral amplitude. 16-APSK (2-ring constellation) with optimized ring radii was found to outperform square 16-QAM and 16-PSK for different baud rates up to 6 GBaud (24 Gb/s). We then studied the joint spectral phase, spectral

Optics EXPRESS

magnitude and eigenvalue modulation and conclude that modulating the real part of the eigenvalue is more bandwidth efficient than modulating the imaginary part of the eigenvalue in practical settings. Moreover, modulating the real part of the eigenvalue induces timing shifts of the soliton pulses which led to interactions with neighboring pulses or nonlinear ISI as the signal propagates along the fiber. To mitigate such distortions, we proposed a timing pre-shift method based on appropriate scaling the spectral magnitude and a record transmission of 4 GBaud 6 bit/symbol (total 24 Gb/s) over 1000 km was demonstrated. The results presented herein laid down another crucial step towards realizing high speed nonlinear fiber transmissions based on nonlinear Fourier Transform. Nonetheless, the constellation designs and signal processing strategies derived are rather preliminary and in-depth analytical investigations and systematic optimizations to improve NFT transmission performance are to be undertaken in the future.

Funding

General Research Fund of the Research Grants Council, Hong Kong (number PolyU152116/15E).

158.132.181.185 {ts '2022-10-19 05:18:14'}